Non-linear impedance boundary condition from linear piecewise B-H curve applied to induction heating systems

Abstract

Purpose – This paper aims to apply the non-linear impedance boundary condition for a linear piecewise B-H curve in frequency domain simulations to find the equivalent impedance of a simple induction heating system model.

Design/methodology/approach – An electromagnetic description of the inductor system is performed to substitute the effects of the induction load, for a mathematical condition, the so-called impedance boundary condition. This is suitable to be used in electromagnetic systems involving high conductive materials at medium frequencies, as it occurs in an induction heating system.

Findings – A reduction of the computational cost of electromagnetic simulation through the application of the impedance boundary condition. The model based on linear piecewise B-H curve simplifies the electromagnetic description, and it can facilitate the identification of the induction load characteristics from experimental measurements.

Practical implications – This work is performed to assess the feasibility of using the nonlinear boundary impedance condition of materials with linear piecewise B-H curve to simulate in the frequency domain with a reduced computational cost compared to time domain simulations.

Originality/value – In this paper, the use of the nonlinear boundary impedance condition to describe materials with BH curve by segments, which can approximate any dependence without hysteresis, has been studied. The results are compared with computationally more expensive time domain simulations.

Keywords Electromagnetism, induction heating, electromagnetic modeling, home appliances.

Paper type Research paper.

Introduction

Domestic induction systems usually work with a simple rectifier which transforms the mains at 50-60 Hz into a modulated DC-bus and, then, a resonant inverter generates an AC current with a frequency ranging from 20 to 100 kHz. In the design process, the inductor system is viewed as an electrical equivalent impedance, $Z_{\text{coil}} = R + j\omega L$ (Acero et al., 2010). This model usually assumes linear magnetic materials. However, the ferromagnetic materials used as a load present saturation, presenting two main non-linear effects: the response $v(t)$ changes with the amplitude of $i(t)$ and a harmonic distortion of the waveform appears. The equivalent impedance of the inductor-load system $Z_{\text{coil}}\left(\omega, \hat{I}\right)$ will be defined by the ratio between the first harmonic of the voltage, V_1, and the current, I_1, considering the classical frequency dependence as well as the current amplitude dependence associated with the non-linearity of the load.

The equivalent impedance can be calculated by using numerical methods, i.e., commercial finite element analysis tools. However, rapid decaying fields into the induction load requires a finer mesh of the load which implies a high computational cost to carry out the simulation of the system. With the purpose to speed up frequency domain simulations, the application of the impedance boundary condition (IBC) avoids the need for meshing the load under certain conditions (Carretero et al., 2011), e.g., characteristics size in the system are larger than the skin depth (δ) in the load at the working frequency of the system. The impedance boundary condition obeys a well-known expression for linear materials but magnetic saturation on the load increases the complexity to define properly the IBC. The problem of extending the IBC to non-linear materials has been studied by previous works. An analytical model for deriving eddy current losses in magnetic materials in deep saturation appears in (Agarwal, 1959). The nonlinear impedance boundary condition is estimated by applying a correction factor with respect to the linear IBC in (Del Vecchio & Ahuja, 2013) or by weighting linear and deep saturation IBCs (Guérin & Meunier, 1996; Krähenbühl et al., 1997). Other strategies based on layered media are given in (Canova et al., 2009; Cruciani et al., 2020; Feliziani et al., 2018). Finally, an approach based on time domain 1-D finite element to calculate the nonlinear IBC is provided in (Sabariego et al., 2010).

In this paper, the non-linear IBC associated with linear piecewise B-H curve will be numerically calculated by applying the finite difference method to the 1-D equation governing the diffusion of the magnetic field into the load material. The core of this work is the extraction of the nonlinear IBC in the frequency domain by extracting the values from the first harmonic of the tangential electric field at the boundary between media obtained by means of 1-D simulation in the time domain. This non-linear IBC will be applied to accurately calculate the equivalent impedance of a reference induction heating system under different excitation levels in the frequency domain regime. Finally, a comparison with computational expensive time-domain results will be performed to prove the feasibility of the proposed method.

Induction system model

Non-linear impedance boundary condition

In a scenario involving a varying magnetic field near a non-perfect conducting material, the electric and magnetic fields penetrate the material a short distance because exhibit an exponential decaying governed by the skin depth (δ). Under certain conditions, the ratio of the tangential components of the electric and magnetic fields at the boundary of the conducting material is equal to a constant called Impedance Boundary Condition (IBC). The application of the IBC to a conductive material is sufficient to determine a unique solution to the system avoiding the simulation of the fields inside the conductor.

The IBC possesses a close expression when the materials have a linear constitutive relationship. In this case, the results of substituting the conductor domain with this boundary condition are accurate when the skin depth is sufficiently small compared to dimensions of the system.

At typical operating frequencies of induction heating systems, it is worthwhile to neglect the radiative effects, i.e., the quasi-static approach is assumed. In that case, the magnetic field inside a medium obeys the following equation (Enokizono & Tanabe, 1995; Jufer & Apostolides, 1976).

$$\frac{1}{\sigma}\nabla^2 H = \frac{\partial B}{\partial t}. \tag{1}$$

A strong decay of fields occurs near the surface of a conductive medium as they penetrate the material, thus, the plane-wave assumption is adopted here to use the approximated laplacian $\nabla^2 H \approx \partial^2 H / \partial z^2$, and we have:

$$\frac{1}{\sigma}\frac{\partial^2 H}{\partial z^2} = \frac{\partial B}{\partial H}\frac{\partial H}{\partial t}. \tag{2}$$

The expression of the impedance boundary condition for a linear material, Z_{IBC}, can be easily derived by solving the preceding equation for a harmonic transverse magnetic field $H(z=0) = H_0 e^{j\omega t}$, where H_0 is the magnetic field amplitude at the surface and ω is the angular frequency. In a linear material, the relationship $\partial B / \partial H = \mu$ is fulfilled. Thus, the magnetic field inside the material obeys:

$$H(z,t) = H_0 e^{-(1+j)z/\delta} e^{j\omega t}, \tag{3}$$

where $\delta = \sqrt{2/\omega\mu\sigma}$ is the skin depth. The transverse electric field can be found by using Ohm's Law and Ampère's Law:

$$E_x(z,t) = -\frac{1}{\sigma}\frac{\partial H_y}{\partial z} = \frac{1+j}{\sigma\delta} e^{-(1+j)z/\delta} e^{j\omega t}. \tag{4}$$

From (3) and (4), the IBC expression for a linear material can be easily derived, (Beggs et al., 1992):

$$Z_{\mathrm{IBC}} = \left.\frac{E_x}{H_y}\right|_{z=0} = \frac{1+j}{\sigma\delta}. \tag{5}$$

This relationship in (5) is well-known and implemented in commercial simulation tool for frequency domain simulations, e.g., COMSOL Multiphysics, (COMSOL Multiphysics Reference Manual, Version 6.0). The solution of the equation is more complicated for non-linear magnetic material, and it is necessary to use numerical methods for almost any B-H curve dependence. In the latter case, the equation (2) can be rearranged as the partial differential equation (PDE):

$$\frac{\partial H}{\partial t} = \frac{1}{\sigma\mu_{\mathrm{diff}}(H)}\frac{\partial^2 H}{\partial z^2}, \tag{6}$$

where $\mu_{\mathrm{diff}}(H) = \partial B(H) / \partial H$ is the differential magnetic permeability. The preceding non-linear 1D diffusion equation can be solved by applying numerical methods. Then, the field dependent impedance boundary condition can be obtained by weighting the solution, as it is given in (Cirimele et al., 2016). However, due to the IBC is typically employed in frequency domain simulation, we have adopted the

definition of the non-linear IBC based on the ratio of the first harmonic of the fields, i.e., higher harmonic distortion is neglected, using the Fourier Transform (Elliot, 1987) because the higher order harmonics are considerably smaller, but including the dependence of the non-linear IBC on the tangential H-field level (Carretero et al., 2024):

$$Z_{\mathrm{IBC}}^{\mathrm{NL}}\left(H_y\right)=\left.\frac{E_x^1}{H_y}\right|_{z=0}. \tag{7}$$

B-H curve model

This paper focuses on obtaining the non-linear IBC of a B-H curve defined linear piecewise. The usefulness of this approach resides in its versatility, as it can be adjusted to any type of curve. This description of B-H curve is equivalent to provide N values of relative permeability μ_r^i for each interval H_s^{i-1} to H_s^i:

$$\mu_{\mathrm{diff},r}=\mu_r^i \quad \text{if} \quad H_s^{i-1}<\left|H\right|<H_s^i, \tag{8}$$

where $i=1,...,N$, $H_s^0=0$ A/m, $H_s^N=H_{\max}\to\infty$ and $\mu_{\mathrm{diff},r}=\frac{1}{\mu_0}\frac{\partial B}{\partial H}$ is the differential relative permeability. The B-H curve associated with the preceding differential permeability can be easily found by integration.

With the purpose to assess the performance with respect to the number of segments *N* on the linear piecewise B-H curve, it is proposed to use as a reference the curve corresponding to the anhysteretic Jiles-Atherton model (Jiles & Atherton, 1986) with a null mean field parameter $\alpha=0$ or Langevin function, whose magnetization field $M\left(H\right)$ is given as follows:

$$M\left(H\right)=M_s\left(\coth\left(\frac{H}{a}\right)+\frac{a}{H}\right). \tag{9}$$

Number of segments *N*	μ_r^i	H_s^i (A/m)
2	948.35, 1.09	1661
3	948.35, 55.71, 1.09	1215, 8948
4	948.35, 227.9, 11.25, 1.09	893.5, 3388, 19289
5	948.35, 292.2, 37.34, 3.57, 1.09	828.1, 2029, 8131, 96205

Table I. Parameters of the linear approximation of the anhysteretic Jiles-Atherton B-H curve.

(Source: Authors' own)

The parameters $a=560$ A/m and $B_s=\mu_0 M_s=2$ T, which correspond to a typical iron. The B-field obeys the constitutive relationship $B\left(H\right)=\mu_0\left(H+M\left(H\right)\right)$ which is fitted to a linear piecewise B-H curve with an increasing number of segments N using a least squares algorithm and enforcing the tangentially condition to equate the relative permeability at $H=0$ and $H_{\max}=10^5$ A/m, respectively, reducing the problem to find just 2*N*-2 parameters. The results of the fit are shown in the Table I.

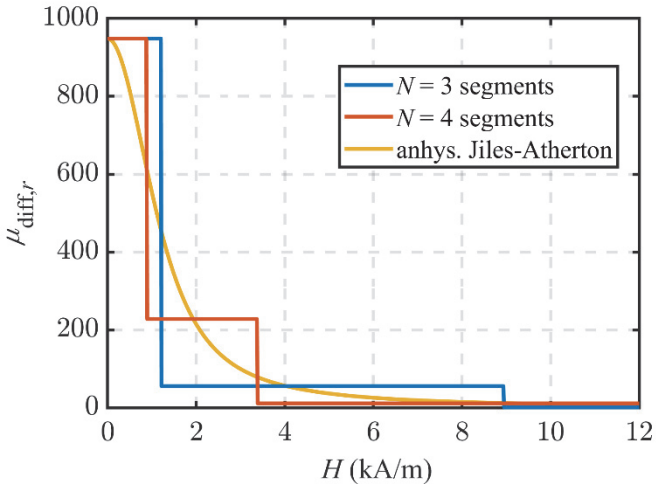

(a)

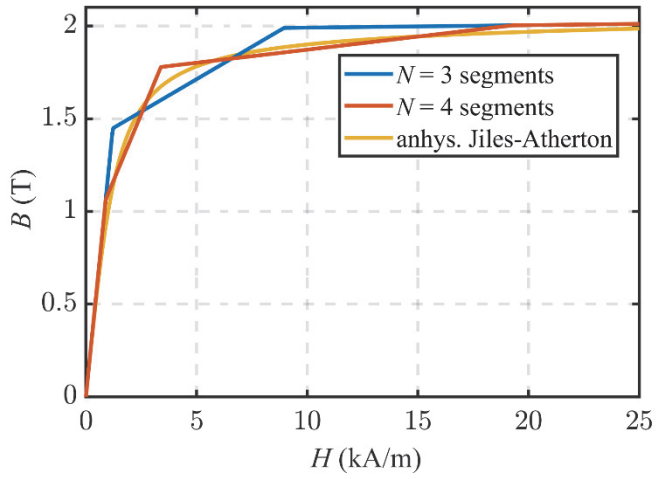

(b)

Figure 1. Comparison of anhysteretic Jiles-Atherton and linear piecewise B-H curves: (a) differential permeability vs *H*-field, (b) *B*-f

The comparison between the anhysteretic Jiles-Atherton B-H curve and some of the linear piecewise B-H curves are shown in Fig. 1. As it can be observed, accuracy of the fitting increases with number of segments N but the main difficult in practical applications is matching the small field range.

Numerical extraction of non-linear impedance boundary condition

In order to find the non-linear IBC, we use finite difference method to solve (6). A non-uniform mesh is implemented using the discretization described in (Jufer & Apostolides, 1976) to save computational cost, but an implicit Euler method is applied in this work guarantying the stability conditions.

In each iteration is necessary to solve a linear system of n equations, where n is the number of spatial nodes along the z-axis, orthogonal to the H-field. LU algorithm optimized for tridiagonal matrices is used for this purpose. The selection of this algorithm implies a large computational cost reduction of $\sim O(n)$ instead of $\sim O(n^2)$ for the standard built-in method in MATLAB®. The boundary conditions applied are:

$$\begin{cases} H_y\left(z=0\right)=H_0\sin\left(\omega t\right) \\ H_y\left(z=z_{\max}\right)=0 \end{cases}. \tag{10}$$

The configuration used for the numerical solution of the PDE consists of a mesh uniformly spaced from $z=0$ to $z=10^{-4}$ m in intervals of $\Delta z=10^{-7}$ and logarithmically spaced from that point to $z_{\max}=10^{-2}$ m with 1000 nodes. The selected time step is such that each period of the external field is divided in 2000 steps: $\Delta t=10^{-3}\pi/\omega$. This mesh was selected by studying the behaviour of the solution with a reference frequency of 50 kHz and a description of the $M\left(H\right)$ curve given by the Langevin function with a saturation of $B_s=2$ T. The electric field on the surface is determined from $E_x=-\frac{1}{\sigma}\left(\frac{\partial H_y}{\partial z}\right)$ using a second order approximation of the derivative. The differential equation has been solved by means of the corresponding code in MATLAB.

It is remarkable that if the mesh is too coarse in points where the magnetic field still has a considerable amplitude, $H_0=10^5-10^6$ A/m, the solution of the electric field on the conductor surface shows spurious. For linear materials or amplitudes in the range of quasi-linear behaviour, the skin depth is independent of the external field amplitude. However, for non-linear magnetic materials, the skin depth increases with the amplitude, effect that must be considered in the selection of the meshing parameters.

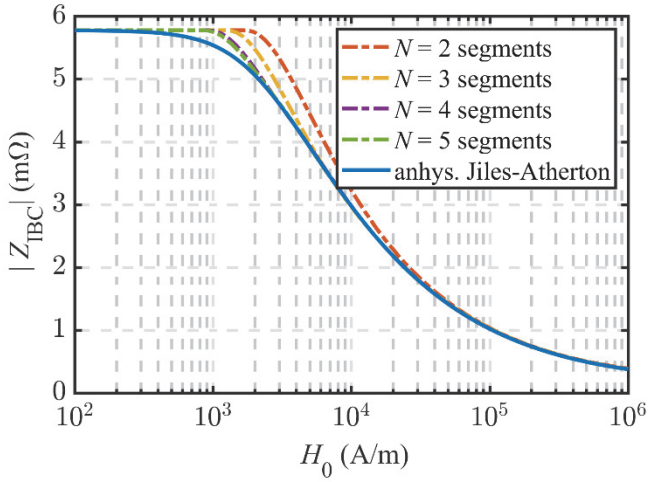

(a)

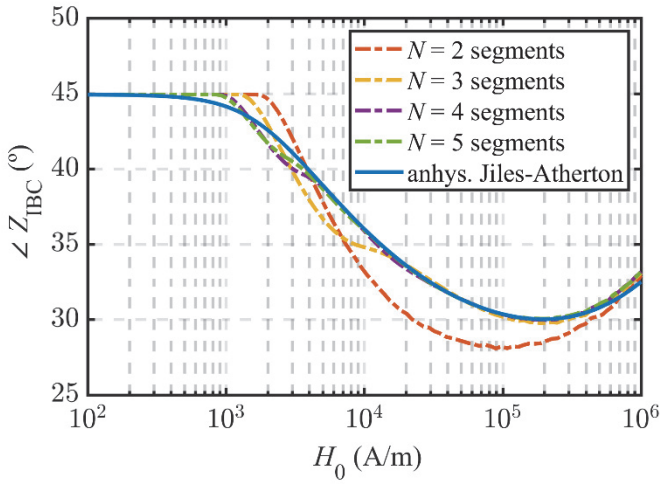

(b)

Figure 2.
Non-linear IBC for different number of pieces of the linear piecewise B-H curve at the frequency of 50 kHz: (a) absolute value, (b) phase of the complex value.

After 8 periods, the relative error between two consecutive periods is less than 0.1% for the reference configuration, consequently, we assume that the steady state has been reached in that moment. Finally, the last period is considered and the Fourier Transform is computed to find the first harmonic and calculate the IBC, as appears in (7). The results are shown in Fig. 2, where non-linear IBC of linear piecewise B-H curve is equal to the linear IBC at small levels of magnetic field, but at higher excitation levels, the non-linear IBC decreases and its real part becomes more important than the imaginary contribution.

FEA-tool simulation model

The simulated induction heating system is a simple axisymmetric model in COMSOL®, as it can be seen in Fig. 3, where the coil is modelled as an azimuthal current density $J(t) = J_0 \sin(\omega t)$, with $J_0 = NI_0/S_{\text{coil}}$ where I_0 is the electrical current amplitude, N the number of turns in the coil and S_{coil} is the coil cross-sectional area. The model is simulated in the frequency-domain regime.

The coil consists of 48 turns uniformly distributed between the internal and external radii of 10 mm and 30 mm, respectively, and the thickness is equal to 4 mm. The flux concentrator is a high permeability plane placed 1 mm beneath the coil, but modelled by a perfect magnetic material. The load is located at a distance of 4 mm above the coil. The conductivity of the load is $\sigma = 1.12 \cdot 10^7$ S/m.

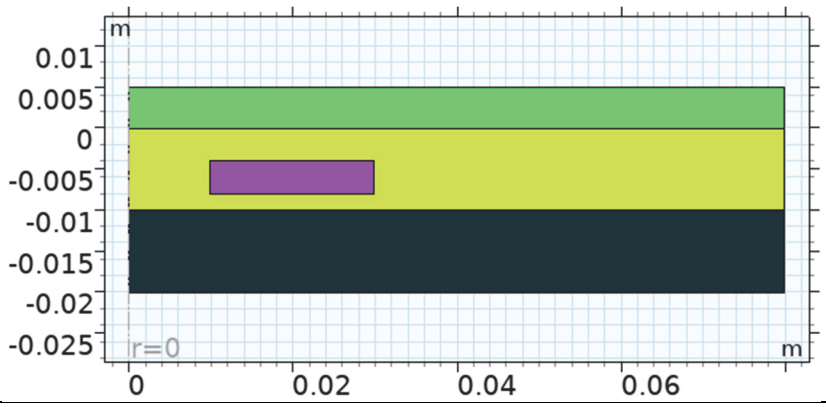

Figure 3.
2D COMSOL® model with axial symmetry (grey: flux concentrator; purple: coil; yellow: air; green: load).

The frequency-domain simulation in COMSOL® is performed with the load of the induction heating system modelled by the non-linear IBC $\left(Z_{\mathrm{IBC}}^{\mathrm{NL}}\right)$. In this kind of simulation, the fields are assumed to be harmonic, which is not totally true due to the existence of higher harmonics, but those are considerably smaller. For this purpose, an equivalent relative permeability is defined:

$$\mu_{\mathrm{eq}}\left(H_0\right)=\frac{2\sigma}{\omega}\left(\frac{Z_{\mathrm{IBC}}^{\mathrm{NL}}\left(H_0\right)}{1+j}\right)^2. \tag{11}$$

This tangent H-field dependent complex-valued equivalent permeability, $\mu_{\mathrm{eq}}\left(H_0\right)$, is inserted into the frequency domain simulation in COMSOL as a characteristic property of the load material. For this purpose, first, the value $\mu(H_0)$ is stored in a lookup table which associates a complex permeability value for each H-field value. For other intermediate H field values, a cubic interpolation will be applied. Finally, COMSOL directly applies the nonlinear boundary impedance condition by inserting the above interpolated tangent H-field dependent complex permeability function into the IBC permeability field.

The voltage in the coil is calculated by integrating the electric field around the coil, taking advantage of the axial symmetry of the system, (Carretero et al., 2012).

$$V_{\mathrm{coil}}\left(\omega,I_0\right)=\frac{n}{S_{\mathrm{coil}}}\int_{S_{\mathrm{coil}}}2\pi r E_{\varphi}\left(\omega,I_0\right)dS, \tag{12}$$

where $V_{\mathrm{coil}}\left(\omega,I_0\right)$ is the amplitude of the induced voltage in the coil at the angular frequency ω and current amplitude I_0, and $E_{\varphi}\left(\omega,I_0\right)$ is the azimuthal component of the electric field extracted from the frequency domain simulation.

The equivalent impedance of the inductor, Z_{coil}, depends on the frequency, f, as well as on the current amplitude, I_0:

$$Z_{\mathrm{coil}}\left(\omega,\hat{I}\right)=\frac{V_{\mathrm{coil}}}{I_0}=R\left(\omega,\hat{I}\right)+j\omega L\left(\omega,\hat{I}\right), \tag{13}$$

Time-domain simulations

The accuracy of the frequency domain simulation, using the proposed nonlinear impedance boundary condition, has been analyzed by comparison with time domain simulations.

In order to capture the fast decay of the fields in time-domain simulation, a logarithmically spaced points mesh is applied to the load. The magnetic properties of the load correspond to the dependence given by the anhysteretic Jiles-Atherton model used to calculate the non-linear IBC in the previous section. The system is simulated for 4 periods because the steady-state is reached then and the computational cost is limited.

The equivalent impedance of the inductor, is calculated by applying a similar equation to (13):

$$Z_{\text{coil}}\left(\omega,\hat{I}\right)=\frac{V_1}{I_0}=R\left(\omega,\hat{I}\right)+j\omega L\left(\omega,\hat{I}\right), \tag{14}$$

where V_1 is the first harmonic of the voltage in the coil. I that case, the first harmonic is extracted by applying the Fourier Transform to the waveforms of the last period in the time-domain simulation, whereas, in frequency-domain simulation, these values are directly provided by the solution variables.

From the simulation of the configurations described in the next section, it can be seen that the computational cost of time-domain simulations increases linearly with the amplitude and presents many convergence problems. Non-linear IBC-based simulation in the frequency domain converges faster with field amplitudes within the linear dependence range, but does not depend on amplitude at higher values.

The computation time per amplitude and frequency for the frequency-domain simulation is $1,45\pm0,06$ s with a reference computer Lenovo IdeaPad S145 (Intel Core i5), which represents approximately a reduction factor of 500 in comparison to time-domain simulation. Thus, in regard to computational cost and simulation convergence, the benefit of using non-linear IBC modelling is evident.

Comparison of equivalent impedance results

In Fig. 4 are represented the comparison of the equivalent resistance and inductance calculated by using non-linear IBC in the frequency-domain regime and full time-domain simulations, respectively, varying the excitation current at selected frequencies. As it can be seen, the agreement between the results is good.

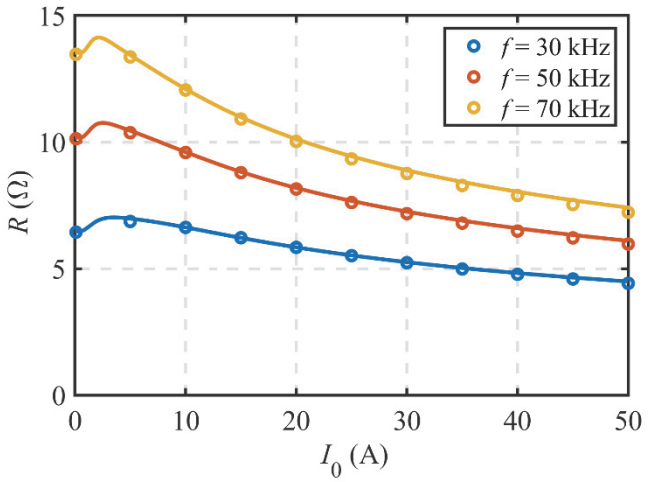

(a)

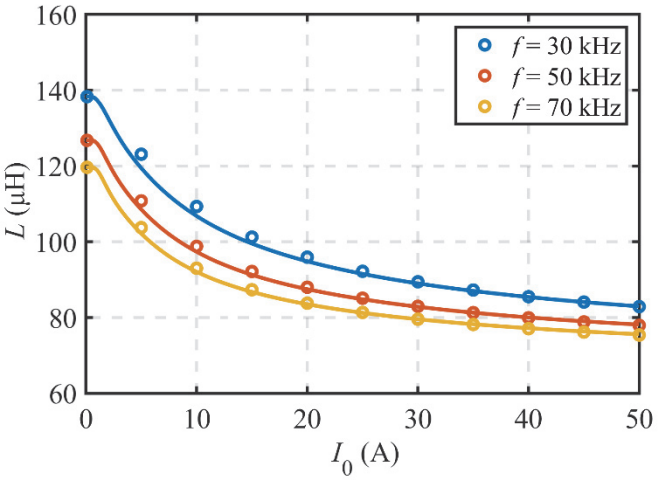

(b)

Figure 4. Equivalent impedance at different current levels (lines: 4-segment B-H curve non-linear IBC results; circles: Jiles-Atherton time-domain results): (a) resistance, (b) inductance.

In Fig. 5 are also depicted the comparison of the equivalent resistance and inductance calculated varying the frequency at selected values of the excitations current. In that case, it can be observed a very good agreement for the small signal level as well as higher current excitation levels, being the accuracy of good quality for intermediate current levels.

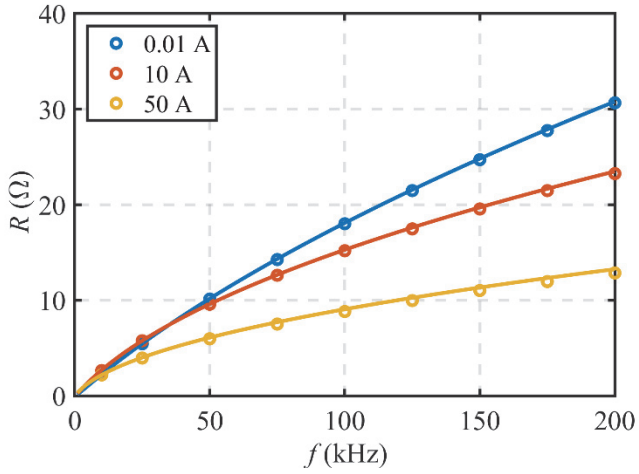

(a)

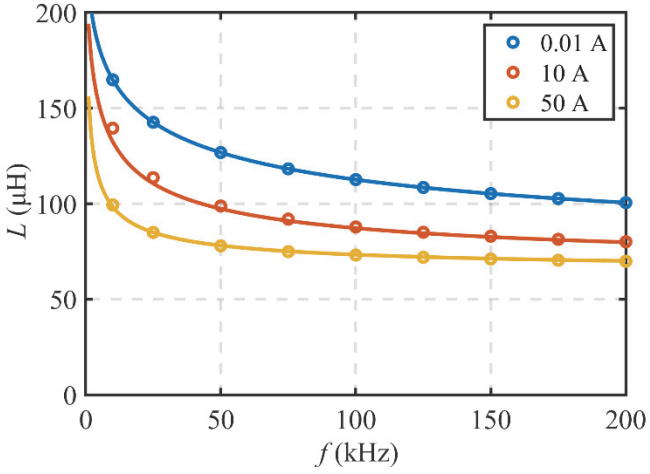

(b)

Figure 5. Equivalent impedance at different frequencies (lines: 4-segment B-H curve non-linear IBC results; circles: Jiles-Atherton time-domain results): (a) resistance, (b) inductance.

Conclusions

In this paper, the potential of the extraction of the non-linear IBC by modelling the B-H curve of a material by a linear piecewise function has been tested. The validity of this approach has been proven by reaching a maximum error limited to 5% in the calculation of the equivalent impedance of the reference induction system, which corresponds to a simplified structure of an induction cooking system. The proposed model extends the dependence on the equivalent impedance of induction heating system to also include current level dependence.

It should be noted that the model based on linear piecewise B-H curve simplifies its description, and it can facilitate the identification of the induction load characteristics from experimental measurements.

References

Acero, J., Burdio, J. M., Barragan, L. A., Navarro, D., Alonso, R., Ramon;, J., Monterde, F., Hernandez, P., Llorente, S., & Garde, I. (2010). An overview of recent research in sarcoma. *IEEE Industry Applications Magazine*, *16*(2), 39–47.

Agarwal, P. D. (1959). Eddy-current losses in solid and laminated iron. *Transactions of the American Institute of Electrical Engineers, Part I: Communication and Electronics*, *78*(2), 169–181.

Beggs, J. H., R. J. Luebbers, Yee, K. S., & Kunz, K. S. (1992). Finite-difference time-domain implementation of surface impedance boundary conditions. *IEEE Transactions on Antennas and Propagation*, *40*(1), 49–56.

Canova, A., Dughiero, F., Fasolo, F., Forzan, M., Freschi, F., Giaccone, L., & Repetto, M. (2009). Identification of equivalent material properties for 3-D numerical modeling of induction heating of ferromagnetic workpieces. *IEEE Transactions on Magnetics*, *45*(3), 1851–1854. https://doi.org/10.1109/TMAG.2009.2012830

Carretero, C., Acero, J., & Burdio, J. M. (2024). Normalized nonlinear impedance boundary condition in anhysteretic magnetic material for eddy current problems. *IEEE Transactions on Magnetics*, *Accepted for publication*.

Carretero, C., Lucia, O., Acero, J., Alonso, R., & Burdio, J. M. (2011). An application of the impedance boundary condition for the design of coils used in domestic induction heating systems. *COMPEL - The International Journal for Computation and Mathematics in Electrical and Electronic Engineering*, *30*(5), 1616–1625.

Carretero, C., Lucia, O., Acero, J., Alonso, R., & Burdio, J. M. (2012). Frequency-dependent modelling of domestic induction heating systems using numerical methods for accurate time-domain simulation. *IET Power Electronics*, *5*(8), 1291–1297.

Cirimele, V., Freschi, F., Giaccone, L., & Repetto, M. (2016). Finite Formulation of Surface Impedance Boundary Conditions. *IEEE Transactions on Magnetics*, *52*(3), 1–4. https://doi.org/10.1109/TMAG.2015.2490102

COMSOL Multiphysics Reference Manual, version 6.0. (n.d.).

Cruciani, S., Campi, T., Maradei, F., & Feliziani, M. (2020). Finite-element modeling of conductive multilayer shields by artificial material single-layer method. *IEEE Transactions on Magnetics*, *56*(1), 1–4. https://doi.org/10.1109/TMAG.2019.2949737

Del Vecchio, R. M., & Ahuja, R. (2013). Analytic nonlinear correction to the impedance boundary condition. *IEEE Transactions on Magnetics*, *49*(12), 5687–5691.

Elliot, D. F. (1987). Transforms and Transform Properties. In D. F. Elliott (Ed.), *Handbook of Digital Signal Processing* (pp. 1–53). Academic Press. https://doi.org/10.1016/b978-0-08-050780-4.50006-0

Enokizono, M., & Tanabe, H. (1995). Numerical analysis of high-frequency induction heating including temperature dependence of material characteristics. *IEEE Transactions on Magnetics*, *31*(4), 2438–2444.

Feliziani, M., Cruciani, S., Campi, T., & Maradei, F. (2018). Artificial Material Single Layer to Model the Field Penetration Through Thin Shields in Finite-Elements Analysis. *IEEE Transactions on Microwave Theory and Techniques*, *66*(1), 56–63. https://doi.org/10.1109/TMTT.2017.2737994

Guérin, C., & Meunier, G. (1996). Surface impedance for 3d non-linear eddy current problems - application to loss computation in transformers. *IEEE Transactions on Magnetics*, *32*(3 PART 2), 808–811.

Jiles, D. C., & Atherton, D. L. (1986). Theory of ferromagnetic hysteresis. *Journal of Magnetism and Magnetic Materials*, *61*(1–2), 48–60.

Jufer, M., & Apostolides, A. (1976). An analysis of eddy current and hysteresis losses in solid iron based upon simulation of saturation and hysteresis characteristics. *IEEE Transactions on Power Apparatus and Systems1*, *PAS-95*(6), 1786–1794.

Krähenbühl, L., Fabrègue, O., Wanser, S., De Sousa Dias, M., & Nicolas, A. (1997). Surface impedances, BIEM and FEM coupled with 1D non linear solutions to solve 3D high frequency eddy current problems. *IEEE Transactions on Magnetics*, *33*(2 PART 2), 1167–1172.

Sabariego, R. V., Dular, P., Geuzaine, C., & Gyselinck, J. (2010). Surface-impedance boundary conditions in dual time-domain finite-element formulations. *IEEE Transactions on Magnetics*, *46*(8), 3524–3531. https://doi.org/10.1109/TMAG.2010.2043234